Quantum Information From Selected Elementary Chemical Reactions: Maximum Entangled Transition State

Rodolfo O. Esquivel,[a,b] Moyocoyani Molina-Espíritu,[a] A. R. Plastino,[b,c] and Jesus S. Dehesa*[b]

Quantum entanglement features exhibited by the reaction path of some selected elementary chemical reactions: hydrogenic abstraction, nucleophilic hydrogenic substitution, three-atom insertion reaction of silylene into hydrogen, and the cycloaddition of cyclopentadiene into anhydride maleic are investigated in this work. The phenomenological behavior of these reactions is described by two of the fundamental descriptors of the molecular densities, the atomic charges, and the electric potentials, to associate the maximum entangled transition state (METS) to the concurrent processes of the chemical reactions. It is found that the METS characterizes the transition state of symmetrical reactions; and for nonsymmetrical ones, it features a new critical point along the intrinsic reaction path. In addition, benchmark calculations of the relevant quantitative entanglement measures for the critical points of these reactions are reported. © 2015 Wiley Periodicals, Inc.

DOI: 10.1002/qua.24926

Introduction

Quantum mechanics constitutes the fundamental backbone behind the theoretical study of molecular systems and chemical reactions.[1] The quantum-mechanical approach to chemical phenomena usually deals with very complex numerical algorithms for the approximate solution of the many-body Schroedinger equation describing a given chemical system. These methods generate orbital representations of the wavefunctions, and the concomitant energy properties that, in turn, assist the qualitative interpretation of chemical phenomena and provide predictive capability. A complementary framework of theoretical research has arisen from the application of tools from Shannon's classical information theory (IT)[2,3] to the analysis of diverse aspects of the probability densities associated with quantum wavefunctions.[4–6] In the contexts of molecular physics and quantum chemistry, this approach allows to interpret chemical structures and phenomena through the information content of the electron densities in conjugated spaces (position and momentum).[7] Significant advances in the interpretation of elementary chemical reactions have been achieved by the use of Shannon entropies to study the localized/delocalized features of the electron density distributions. This provides a phenomenological description of the course of elementary chemical reactions that reveals important stages in these processes that are not easily detected in the energy profile, such as the ones in which bond forming and bond breaking occur.[8] As well, the synchronous reaction mechanism of a S_N2 type chemical reaction and the nonsynchronous mechanistic behavior of the simplest hydrogenic abstraction reaction were predicted by use of Shannon entropies analysis.[9] Besides, complexity measures have also been used to analyze chemical processes.[10]

Notwithstanding that classical IT has been proven to be useful to interpret several aspects of chemical phenomena, to the best of our knowledge, there are no studies related to quantum IT applied to chemical reactions, that is, to characterize the quantum correlations that arise in the passage from reactants to products. Quantum entanglement is one of the most fundamental aspects of the quantum-mechanical description of nature.[11] Further, entanglement plays a central role in some proposals for the implementation of quantum information technologies. Indeed, some promising schemes for quantum computation rely on the controlled manipulation of entangled states of quantum dots (clusters) or molecules and, therefore, are already within the realm of theoretical chemistry. Furthermore, although the first experiments regarding quantum teleportation have been performed using photons, teleportation with the massive particles chemists deal with is also of great interest.[12] Last, but certainly not least, we should mention the new field of quantum biology,[13] closely related to quantum IT, where chemical phenomena obviously play a crucial role. It is, therefore, clear that important developments related to quantum information are entering the sphere of

[a] R. O. Esquivel, M. Molina-Espíritu
Departamento de Química, Universidad Autónoma Metropolitana, 09340-México D.F., México
[b] R. O. Esquivel, A. R. Plastino and J. S. Dehesa
Computacional and Departamento de Física Atómica, Instituto Carlos I de Física Teórica y, Molecular y Nuclear, Universidad de Granada, 18071-Granada, Spain
E-mail: dehesa@ugr.es
[c] A. R. Plastino
CeBio y Secretaria de Investigaciones, Universidad Nacional Noroeste-Buenos Aires-UNNOBA-Conicet, Roque Saenz-Peña 456, Junin, Argentina

Contract grant sponsor: Professor Jesús S. Dehesa and GENIL-SPR at the Universidad de Granada for financial support during the 2014–2015 period (to R.O.E.).
Contract grant sponsor: Mexican Grant; Contract grant numbers: CONACyT CB-2009-01/132224 and PROMEP-SEP.
Contract grant sponsor: Spanish Grant; Contract grant numbers: FIS2011–24540, FQM-7276, FQM-4643.

interest of chemistry.[14,15] Consequently, it is imperative for both quantum information theorists and theoretical chemists to concern themselves with the entanglement features exhibited by chemical systems and processes.[16]

The motivations for the exploration of the entanglement properties of chemical systems are manyfold. Generally speaking, if two particles are in an entangled state, then even if the particles are physically separated by a large distance, they behave in some respect as a single entity rather than as two separate entities. A natural mechanism generating entanglement takes place when a former unit dissociates into simpler subsystems. This kind of processes is known quite well in chemistry. The study of entanglement in quantum chemistry may also shed new light on the real-space partitioning of a molecule into subsystems, which is still a challenging problem in theoretical chemistry.[17] So, apart from its basic relevance for the foundations of physics, entanglement has to play an important role in chemistry too. Although information entropies have been used for a variety of studies in chemistry,[7] applications of entanglement measures in chemical systems are very scarce. Recently, the connection between entanglement and correlation energy has been studied in the context of a two-electron artificial atom.[18] Studies of the electron correlation and entanglement in the He atom and H_2 molecule have been reported in Refs. [19, 20]. More recently, Benenti et al.,[21] have used a configuration-interaction variational method to compute the von Neumann and the linear entropy for several low-energy singlet and triplet eigenstates of helium. Lin et al.[22] have studied the spacial quantum entanglement of helium-like ions by used of two-electron wavefunctions built by b-spline basis. Also, the entanglement properties of bound states in various two-electron atomic models of Moshinsky, Crandall, and Hooke types were investigated.[23,24] As well, the amount of entanglement of the ground state and of the first few excited states of helium was assessed by using high-quality state-of-the-art wavefunctions.[25] Other interesting results concerning quantum entanglement in atomic and related systems have been reported in Refs. [26–40]. The quantum entanglement-related aspects of the dissociation process of homo- and heteronuclear diatomic molecules have been investigated in Ref. [41]. Conversely, chemical bonding represents a very important concept to understand chemical compounds.[42] Recently, orbital entanglement has been used to qualitative understanding of bond-forming and bond-breaking processes.[43,44] Further, the von Neumann entropy has been used to locate the quantum critical point in low-dimensional spin or fermionic models.[45] Other related tools have been recently used in quantum chemistry to locate transitions in the potential energy curve of the ionic-covalent avoided crossing in LiF[46] and on pseudo-one-dimensional systems to investigate metal-insulator-like transition.[47]

It is of great interest in Chemistry to understand molecular systems as a combination of atoms and molecular fragments. Chemical processes involve small changes between atoms and molecular subsystems and it is crucial to understand the behavior of the classical and quantum-mechanical correlations involved in such chemical changes. Therefore, it is important to analyze the course of chemical reactions at the light of the deeper correlations that arise at the quantum level, that is, by use of the entanglement of a chemical process. It is in the course of chemical processes where entanglement acquires a much deeper sense because of the natural interactions arising among two (or more) subsystems. It must be realized that quantum entanglement is not just a fashionable research topic, it is a fundamental concept of quantum physics that plays a deep role within all applications of quantum mechanics involving composite systems (e.g., problems directly related with molecular systems and chemical processes as mentioned earlier). Although several measures of entanglement have been used recently to characterize atoms in their ground and excited states, as it was mentioned above, this kind of studies have not been undertaken on chemical reactions. The aim of this work is to investigate some aspects of the relationship between quantum entanglement and chemical reactions. The article is organized as follows. In quantum entanglement in molecular systems section, we provide a brief review of the main concepts and tools required for the analysis of entanglement in fermionic systems, and of their application to the study of electronic entanglement in molecules and in chemical reactions. The main results of this work, and the corresponding discussion, are reported in results and discussion section. Finally, some conclusions are drawn in conclusions section.

Quantum Entanglement in Molecular Systems

A quantum entanglement

The state vector of a composite system, consisting of two distinguishable subsystems A and B, is represented by a vector belonging to the tensor product of the two Hilbert spaces $H_A \otimes H_B$. The general state of this system can be written as a linear superposition of products of individual states,

$$\Psi^{AB}=\sum_{m}^{M}\sum_{n}^{N} c_{mn}\omega_m(A)\psi_n(B) \tag{1}$$

where $\{\omega_m(A); m=1,\ldots,M\}$ and $\{\psi_n(B); n=1,\ldots,N\}$ are the basis of the subsystems A and B, respectively. This state can always be decomposed in the Schmidt diagonal form,

$$\Psi^{AB}=\sum_{l}^{r} \lambda_l\chi_l(A)\phi_l(B) \tag{2}$$

where $r=\min(M,N)$ and $\chi_l(A)$ and $\phi_l(B)$ are orthonormal bases for A and B, respectively. Note that in this form, the correlations between the two subsystems are completely revealed. If A is found in the state $\chi_p(A)$, for example, then the state of B is in the $\phi_p(B)$ state. Also note that if $r=1$ the subsystems are not entangled while if $r>1$ they are entangled.

A basic property of entangled pure states of bipartite quantum systems is that it is not possible to assign a pure state to each subsystem individually. Each subsystem is in a mixed state, described by the corresponding marginal density matrix, $\rho_{A,B}=Tr_{B,A}(|\Psi^{AB}\rangle\langle\Psi^{AB}|)$. The amount of entanglement present

in the pure state $|\Psi^{AB}\rangle$ is then given by the degree of mixedness exhibited by these marginal density matrices. Accordingly, the most fundamental measure of entanglement for pure states is given by the von Neumann entropy of the marginal density matrices,

$$E[|\Psi^{AB}\rangle]=S(\rho_{A,B})=-Tr(\rho_{A,B}\ln\rho_{A,B}). \quad (3)$$

Another quantitative indicator of entanglement, that is often used in practical applications is given by the linear entropy of the marginal density matrices,

$$E_L[|\Psi^{AB}\rangle]=S_L(\rho_{A,B})=1-Tr(\rho^2_{A,B}). \quad (4)$$

Entanglement in fermionic systems

Let us consider now a system consisting of N identical fermions having a single-particle Hilbert space of dimension D, with $N \leq D$. A pure state $|\Psi\rangle$ of such a system is separable (nonentangled) if it has Slater rank equal to one. In other words, the state is nonentangled if it can be represented as a single Slater determinant $\det\{|1\rangle, |2\rangle, ...|N\rangle\}$ in an appropriate single particle orthonormal basis $|i\rangle$, $i=1, ...D$. A pure state of the N-fermionic system that cannot be expressed in the above way is endowed with a finite amount of entanglement. This means that correlations between the N fermions that are due solely to the antisymmetric character of the fermionic states do not contribute to the state's entanglement.[48–51] Therefore, the amount of entanglement exhibited by an N-fermion state corresponds, basically, to the quantum correlations that the state has on top of the minimum ones necessary to satisfy the antisymmetric constraint of the fermionic wave function. These considerations lead naturally to the formulation of quantitative indicators of the amount of entanglement exhibited by pure states of N identical fermions. These entanglement indicators are based on appropriate entropic measures evaluated on the single particle reduced density matrix $\rho_r=Tr_{2,...,N}(|\Psi\rangle\langle\Psi|)$ (see Ref. [49] and references therein). One of these entanglement measures is based on the von Neumann entropy. The von Neumann entropy $S[\rho_r]=-Tr(\rho_r\ln\rho_r)$ of the first-order reduced statistical operator ρ_r obeys

$$S[\rho_r] \geq \ln N, \quad (5)$$

with equality verified if and only if the N-fermion pure state has Slater rank one. Then, it is reasonable to regard the difference

$$\xi_{\mathrm{VN}}[|\Psi\rangle]=S[\rho_r]-\ln N \quad (6)$$

as a quantitative indicator (measure) of the amount of entanglement exhibited by a pure state $|\Psi\rangle$ of a system of N identical fermions. As already mentioned, this is a non-negative quantity that vanishes if and only if the state $|\Psi\rangle$ is nonentangled. The term—$\ln N$ appearing in (6) takes into account the fact that even in the separable case (represented by a Slater determinant) the entropy of the first-order reduced density matrix does not vanish and is equal to $\ln N$.

In the particular case of $N=2$, the entanglement measure can be related to the Schmidt decomposition of pure states of two identical fermions. In fact, the Schmidt decomposition admits a natural generalization to systems of two identical particles, supporting the physical meaningfulness of entanglement measures based on entropies evaluated on ρ_r. In the case of pure states of two identical fermions, it is always possible to find an orthonormal basis $\{|i\rangle,\ i=1,2,...\}$ of the single-particle Hilbert space, such that the two-particle pure state $|\Psi\rangle$ can be written as

$$|\Psi\rangle = \sum_i \sqrt{\frac{\alpha_i}{2}}\,(|2i-1\rangle|2i\rangle-|2i\rangle|2i-1\rangle), \quad (7)$$

with $0 \geq \alpha_i \geq 1$ and

$$\sum_i \alpha_i = 1. \quad (8)$$

If the single-particle Hilbert space has a finite dimension D, we assume that D is even and that the sum on the index i appearing in the Schmidt decomposition goes from $i=1$ to $i=D/2$. In terms of the Schmidt basis $\{|i\rangle\}$ and the Schmidt coefficients $\{\alpha_i\}$, the single particle reduced density matrix reads,

$$\rho_r = \sum_i \frac{\alpha_i}{2}(|2i-1\rangle\langle 2i-1|+|2i\rangle\langle 2i|). \quad (9)$$

We see then that the eigenvectors of the reduced density matrix ρ_r are precisely the members of the Schmidt basis, and that the eigenvalues of ρ_r are $\lambda_i=\frac{\alpha_i}{2}$, $i=1,2,...$, each eigenvalue being twofold degenerate. Consequently, the normalization (8) of the Schmidt coefficients is consistent with the fact that the reduced matrix ρ_r is normalized to unity. In terms of this fermionic Schmidt decomposition, the amount of entanglement exhibited by the pure state $|\Psi\rangle$ [as given by (6)] is

$$\xi_{\mathrm{vN}}=S[\rho_r]-\ln 2=-\sum_i \alpha_i \ln \alpha_i \quad (10)$$

where $\rho_r=Tr_2(|\Psi\rangle\langle\Psi|)$ is the first-order reduced density matrix obtained by tracing the global, two-particle density matrix $\rho=|\Psi\rangle\langle\Psi|$ over one of the two particles. The quantitative entanglement indicator ξ_{vN} has been applied to several problems, particularly in connection with two and three-fermion systems.[23,50,51]

An alternative indicator of entanglement for pure states of N identical fermions is based on the linear entropy of the single particle reduced density matrix,

$$S_L[\rho_r]=1-Tr(\rho_r^2). \quad (11)$$

The corresponding entanglement measure is given by,

$$\xi_L[|\Psi\rangle]=N\left[S_L[\rho_r]-\left(\frac{N-1}{N}\right)\right] \quad (12)$$

As happens with the previously discussed measure based on the von Neumann entropy, the entanglement indicator (12) is also a non-negative quantity that vanishes if and only if the state $|\Psi\rangle$ has Slater rank 1 and is, therefore, separable. The constant term appearing within the square brackets in (12) takes into consideration that even for separable (pure) states the linear entropy of the first-order reduced density matrix is not zero and is, instead, equal to $\frac{N-1}{N}$. The overall multiplicative factor N normalizes the entanglement measure to the range [1]. In the special case of systems of two identical fermions ($N=2$), this quantity can be related to the Schmidt decomposition,

$$\xi_L(|\Psi\rangle)=1-\sum_i \alpha_i^2=1-2Tr(\rho_r^2), \quad (13)$$

This entanglement measure (12) has been applied to several problems, particularly in connection with two-fermion systems[23] and also to helium in its ground state and some selected singlet and triplet excited states.[25]

Electronic entanglement in molecules

In this section, we review briefly some quantitative entanglement indicators that are appropriate for studying the electronic entanglement associated with molecules and chemical processes. Let $|\Psi\rangle$ stand for the N-electron quantum state corresponding to a chemical system. As explained before, to evaluate the amount of entanglement exhibited by the state $|\Psi\rangle$ one needs the first-order reduced density matrix ρ_r obtaining by tracing the global density matrix $|\Psi\rangle\langle\Psi|$ over the degrees of freedom of $N-1$ electrons. In the context of quantum chemistry, the first-order reduced density matrix is usually normalized to the total number of electrons N, and its eigenfunctions are called natural spin orbitals, after Löwdin.[52] The associated eigenvalues are the natural spin occupation numbers n_i^γ, $\{n_i^\gamma; i=1,\ldots,M\}$, with M standing for the number of orbitals and γ for the α or β spin majority channels. Note that one deals here with an effective $2M$-dimensional single-particle Hilbert space. One has $0\leq n_i^\gamma\leq 1$ and $\sum n_i^\gamma=N$. Natural spin orbitals are obtained by performing symmetric (orthogonal) transformations on the density matrix so as to obtain its diagonal form characterized by a spectral decomposition representing the symmetry point group of the molecule, unless an atomic partitioning scheme is used.[52]

When computing the amount of entanglement associated with the state of the N electrons it is convenient to normalize the first-order reduced density matrix ρ_r to 1. In that case, the eigenvalues of ρ_r are $\lambda_i^\gamma=n_i^\gamma/N$. Taking this normalization into account, the von Neumann entropy $-Tr(\rho_r\ln\rho_r)$ of the electronic single particle reduced density matrix of a molecular system can be expressed in terms of the natural spin occupation numbers, by recourse to Löwdin's spectral decomposition, as

$$S[\rho_r]=-\sum_{i=1}^{M}\sum_{\gamma=\alpha}^{\beta}\frac{n_i^\gamma}{N}\ln\frac{n_i^\gamma}{N}, \quad (14)$$

where M stands for the dimension of the basis set.

It is worth noticing that closed shell molecular and atomic systems are commonly represented through a $M\times M$ double occupied density matrix $\rho_M^{(DO)}$ with eigenvalues $\lambda_i^{(DO)}$, where $\lambda_i^{(DO)}/2=n_i^\alpha/N=n_i^\beta/N$ and $\sum_i \lambda_i^{(DO)}=1$. Therefore, it is readily seen from (6) that ξ_{vN} can be expressed in an equivalent manner, in terms of $\rho_r^{(DO)}$ as

$$\xi_{vN}[|\Psi\rangle]=S[\rho_r^{(DO)}]-\ln\frac{N}{2}, \quad (15)$$

where

$$S[\rho_r^{(DO)}]=-\sum_{i=1}^{M}\lambda_i^{(DO)}\ln\lambda_i^{(DO)} \quad (16)$$

is the von Neumann entropy of the double occupied density matrix $\rho_r^{(DO)}$. Moreover, these measures, Eqs. (9) and (10), were recently applied to diatomic molecules in their dissociation process.[41]

Similarly to what happens with the von Neumann entropy of ρ_r, for a closed shell molecule the linear entropy of the first-order reduced density matrix ρ_r can be written in terms of the double occupied density matrix $\rho_r^{(DO)}$, as

$$S_L[\rho_r]=1-\frac{1}{2}Tr\left[\left(\rho_r^{(DO)}\right)^2\right]=1-\frac{1}{2}\sum_{i=1}^{M}(\lambda_i^{(DO)})^2, \quad (17)$$

The entanglement measure (12) is then given by

$$\xi_L[|\Psi\rangle]=1-\frac{N}{2}\left(\sum_{i=i}^{M}(\lambda_i^{(DO)})^2\right). \quad (18)$$

Note that Eqs. (15–18) are only valid for closed shell systems, that is, $n_i^\alpha=n_i^\beta$. For open shell systems, one has to use the standard definitions above for each spin channel.

Results and Discussion

The aim of this work is to characterize several elementary chemical reactions from the point of view of quantum information through the entropies and the entanglement measures above described [Eqs. (15-18)]. To calculate these quantities, we have used state-of-the-art wavefunctions from *ab initio* electron structure methods at the post-Hartree–Fock level of theory. In an elementary chemical reaction, some intermediate states might be distinguished. According to the transition state (TS) theory,[53] a chemical reaction ($A+B\rightarrow C+D$) is described by reactants ($\mathbf{R}=\mathbf{A}$ and $\mathbf{B}$) transforming into products ($\mathbf{P}=\mathbf{C}$ and $\mathbf{D}$) by surmounting a potential barrier characterized by the TS. On mathematical grounds, the TS represents a first-order saddle point connecting two minima in a topological sense, and physically it represents a maximum in the potential energy surface (PES) within the space of all possible nuclear

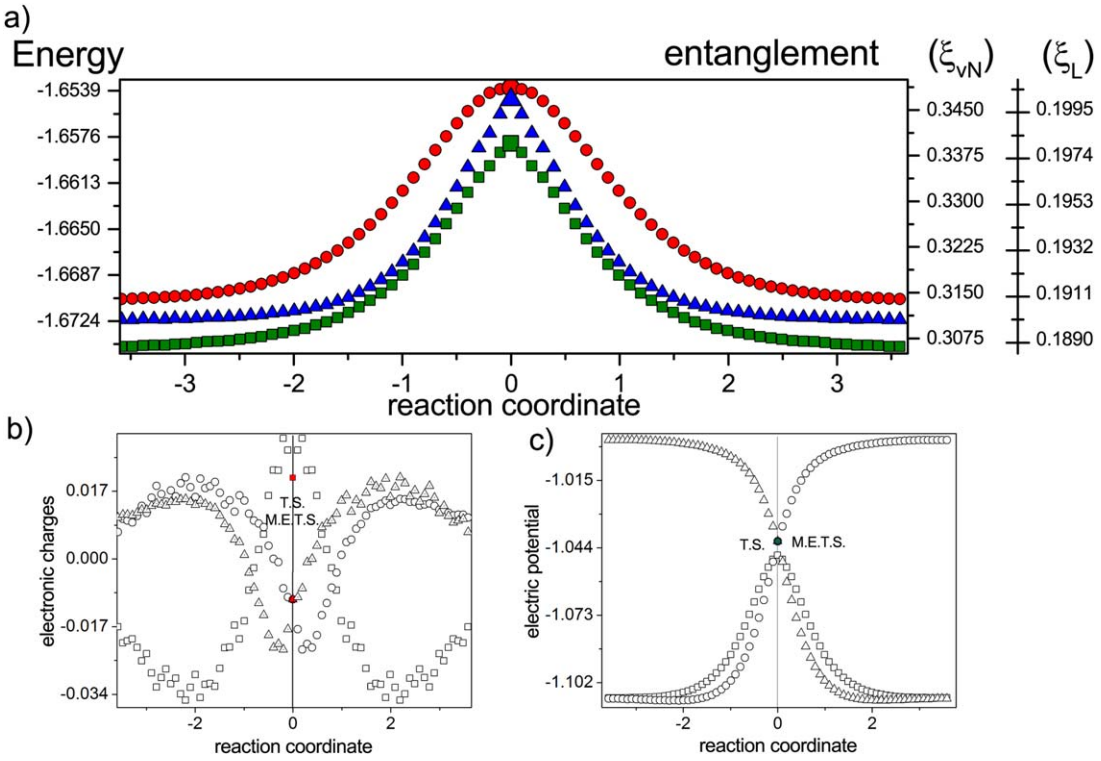

Figure 1. Phenomenological behavior for a) the energy (red) at the **TS** and for the entanglement measures (linear in blue, and von Neumann in green) at the **METS** according to b) the atomic charges (q_i) and c) atomic electric potentials ($\in_i$) for the hydrogenic abstraction reaction intermediates: H(triangles)$\cdots$H$_2$, H$\cdots$H(squares)$\cdots$H, and H$_2\cdots$H(circles).

configurations corresponding to the energetically easiest passage from reactants to products constrained to the Born–Oppenheimer approximation.

To provide with a physical explanation of the behavior of the quantum information-theoretical measures along the course of each of the reaction paths, in particular at their minima and maxima, we have used two fundamental physical descriptors of the molecular densities, the atomic charges as obtained from the molecular electrostatic potential (MEP) and the atomic electric potentials associated with the basins of the MEP (see below). Both properties are good descriptors of the phenomenological behavior of the course of chemical reactions, that is, a higher/lower electric potential (negative) is associated to a lower/higher capacity to gain negative electron charge. Interestingly, bonding situations occur when the difference between the atomic electric potentials of two or more species, either atoms or molecular fragments, become maximum at a specific intrinsic reaction path (IRC) region.[54]

The MEP represents the molecular potential energy of a test charge (proton) at a particular location near a molecule, say at nucleus A. Then, the atomic electrostatic potential, V_A, is defined as

$$V_A=\sum_{B\neq A}\frac{Z_B}{|\mathbf{R}_B-\mathbf{R}_A|}-\int\frac{\rho(\mathbf{r}')d\mathbf{r}'}{|\mathbf{r}-\mathbf{r}'|} \tag{19}$$

where $\rho(\mathbf{r})$ is the molecular electron density and Z_A is the nuclear charge on atom A, located at R_A. Hence, a negative electrostatic potential corresponds to the attraction of the proton by the spatial region of electron molecular density that arises from lone pairs, pi-bonds, and so forth. Positive electrostatic potential corresponds to repulsion of the proton by the atomic nuclei in regions where low electron density exists and the nuclear charge is not completely screened. A charge fitting procedure is used to extract atomic charges from molecular wavefunctions, the MEP is mapped to the electron density that is obtained by use of *ab initio* methods. The nonbonded atomic electric potentials ($\in_i$) along with the fitted atomic charges (q_i) will be used throughout this study according to the CHELPG method.[55] Atomic units are used throughout.

Hydrogenic abstraction reaction

The reaction H$^{\bullet}$+H$_2$ $\rightarrow$ H$_2$+H$^{\bullet}$ is the simplest radical abstraction reaction involving a free radical (atomic hydrogen) as a reactive intermediate. This kind of reaction involves at least two steps. In the first step before the TS, a new radical (atomic hydrogen in this case) is created by homolysis, and in the second one after the TS, the new radical recombines with another radical species.

Our calculations for this reaction were performed in two different steps. First, all the relevant chemical structures for the reaction path from **R** to **P** were obtained at the UMP2/6–311G level of theory,[8] according to the IRC method[56] and the TS theory[53] within the Born–Oppenheimer approximation. Second, all the physical and the quantum information-theoretic quantities for all the chemical structures of the chemical path at the CISD/6-311++G** level of theory. The IRC produced 72 points evenly distributed in the chemical path. As a result, we have plotted in Figure 1a the typical energy profile, for this

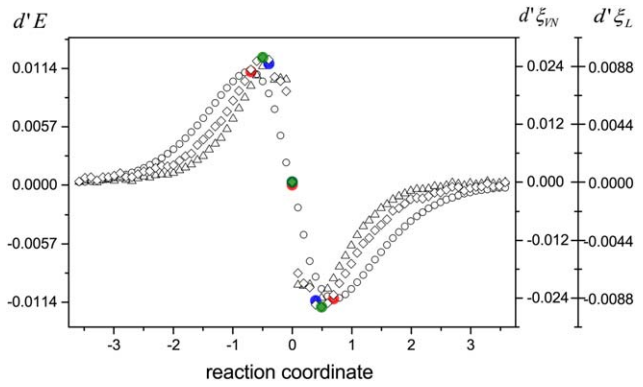

Figure 2. First derivative for the energy profile (circles) and the entanglement measures, linear (squares), and von Neumann (triangles) profile for the hydrogenic abstraction reaction. To guide the eye, colored dots indicate the critical points: energy (red), linear (blue), and von Neumann (green).

reaction, along with the entanglement measures so as to associate the **TS** and the maximum entangled transition state **(METS)** to the concurrent process of equalization of the charges.

From Figure 1a, it is observed that the entanglement measures for the von Neumann entropy [Eq. (15)] and the linear entropy [Eq. (18)] is very similar to that of the energy revealing that the chemical species **R** and **P** possess the lowest values for both entropies as compared with the **TS**, which is in agreement with the chemical intuition, that is, as the reaction progresses from the R, both species **A** and **B** combine in a maximum mixed state which corresponds to the **TS** (maximum energy barrier in Fig. 1a). This is in complete agreement with the significance of a METS. Of course as the reaction path approaches the initial and final states, **R** and **P**, the entanglement measures tend to the separable states.

Physically, we can associate the chemical process according to the change of the atomic charges (q_i; see Fig. 1b): as the reaction progresses from **R** to **P** the charge of the central hydrogenic species (squares) gets more negative at the expense of the entering (triangles) and the leaving ones (circles), which become more positive. This transferring of charge ends at $R_x \simeq -2.0$ where the bond cleavage energy region is reached (BCER, see Ref. [54]) and the entanglement does not show any critical point change at this region other than its monotonic increasing behavior. Beyond this region, the opposite is observed; that is, the entering and the leaving hydrogenic species become more negative at the expense of the central one. This transfer of charge ends at $R_x \simeq -0.5$, where the bond rupture starts between the leaving and the central atomic species (see Ref. [54]). Note that according to Figure 1a, the energy and the entanglement measures show an inflection point signaling this process at each side of the TS. Then, the **TS** is reached at the **METS**), (see Fig. 1a), where local extrema for the atomic charges are observed: a minimum for the central hydrogen and maxima for the leaving and the entering species, see Figure 1b. Note that at this point, a spin coupling process between the atomic species has occurred. It is worth adding that according to the chemical prescription, the **TS** would have an equal probability of forming the reactants or of forming the products of an elementary reaction. This is in complete agreement to what a METS represents, providing in this manner a simple interpretation of a chemical process from the quantum information perspective.

Furthermore, the atomic electric potentials depicted in Figure 1c support the aforementioned phenomena in that as the reaction progresses from the **R** to the **TS** the entering hydrogenic species (triangles) holds a maximum capacity of acquiring electronic charge (tendency for spin coupling) whereas the central and the leaving ones behave in an opposite way, characterizing the beginning of the reaction through this driving force. The tendency diminishes as the reactants approach the **TS** where the electric potential of all atomic species equalize and hence the METS is reached, see Figure 1a. Note that the inflection points for the $\in_i$ of the entering and the leaving species coincide with the minima of the atomic charges wherein the bond breaking process start occurring, see Ref. [54]. Note also that according to Figure 1a, the energy and the entanglement measures show an inflection point at $R_x \simeq -0.5$ where the equalization of the atomic potentials among the central atom and the leaving and entering species occur at each side of the TS.

To the end of analyzing the critical points of the energy profile and that of the entanglement measures, we have depicted the first derivative of these quantities in Figure 2 where it is apparent that an inflection point for these energetic and quantum information-theoretical measures is found at around $R_x \simeq -0.5$.

In Table 1, we have reported the values for all the chemically significant intermediates (**R**, **P,** and **TS**) that are readily apparent from the entropies and the entanglement measures [Eqs. (15)-18)] at the CISD/6-311++G** level of theory.

S_N2: hydrogenic identity substitution reaction

The $H_a^- + CH_4 \rightarrow CH_4 + H_b^-$ represents a typical substitution (S_N2) reaction involving only one step in contrast with the previous reaction (see hydrogenic abstraction reaction subsection) which involves two-steps. It has been observed that this kind of reactions proceed by an inversion TS where the entering

Table 1. Linear and von Neumann entropies and the associated entanglement measures corresponding to **R**, **P,** and **TS** for the hydrogenic abstraction reaction according to Eqs. (15)–(18).

	S_L	ξ_L	S_{vN}	ξ_{vN}
R	7.3001725 E − 01	1.9005714 E − 01	7.1163083 E − 01	3.0617239 E − 01
P	7.3001725 E − 01	1.9005714 E − 01	7.1163083 E − 01	3.0617239 E − 01
TS	7.3336193 E − 01	2.0008312 E − 01	7.4499549 E − 01	3.3952705 E − 01

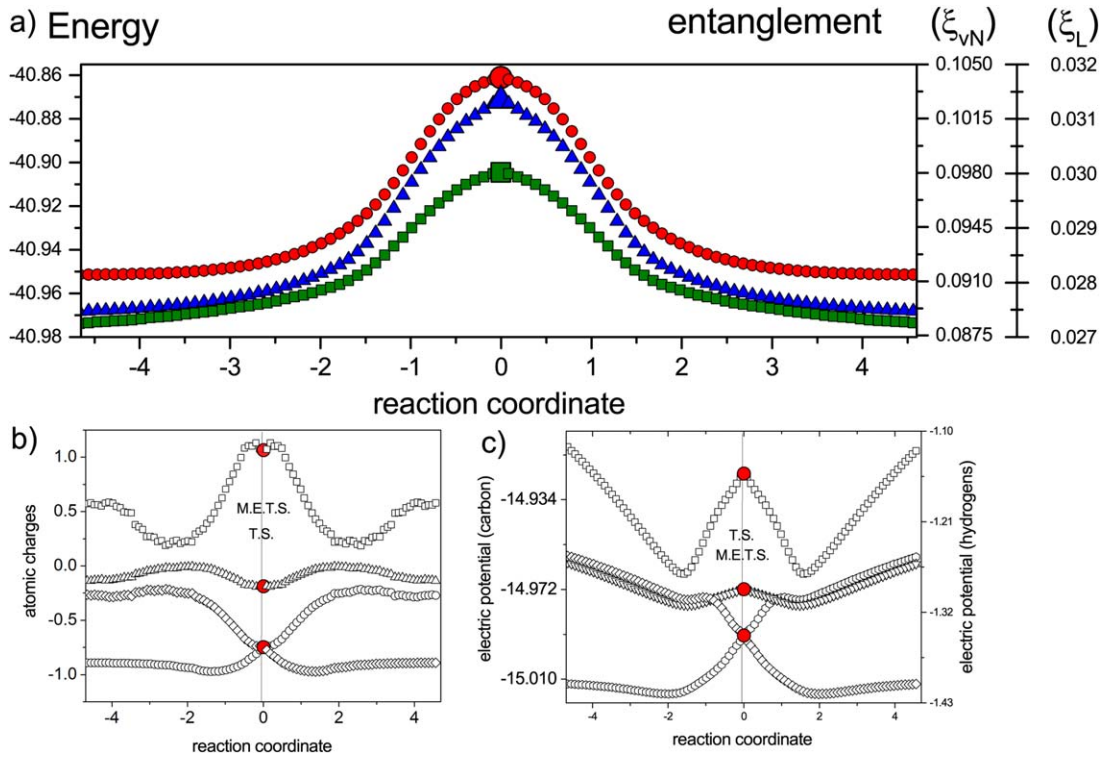

Figure 3. Phenomenological behavior for a) the energy (red) at the **TS** and for the entanglement measures (linear in blue, and von Neumann in green) at the **METS**, according to b) the atomic charges (q_i) and c) atomic electric potentials ($\in_i$) for the S_N2 reaction intermediates: H^-_{enter}(circles)$\cdots CH_3-H_{leave}$, $[H_{enter}\cdots C(squares)-H_3(triangles)\cdots H_{leave}]^-$, and $H_{enter}-CH_3\cdots H^-_{leave}$(diamonds).

species H_a^- displaces the leaving one H_b^- from the backside of the chemical structure in a single concerted reaction step.

The electronic structure calculations for this reaction were performed in an analogous way to that described in hydrogenic abstraction reaction subsection. Calculations for the IRC were performed at the MP2/6-311++G** level of theory, which generated 93 points evenly distributed along the IRC path.[8] Then, the CISD/6-311++G** method was used[56] to calculate all information-theoretic quantities and physical properties (q_i and $\in_i$) for all chemical structures at the IRC path of the S_N2 reaction. The energy profile for this reaction is drawn in Figure 3a, along with the corresponding entanglement measures, so as to associate the **TS** and the **METS** to the concurrent process of equalization of the charges of the entering (circles) and the leaving (triangles) hydrogens, hence for this symmetrical reaction the energy and the entanglement measures possess the same meaning by signaling the same process.

Next, we use the atomic charges of the S_N2 reaction, which have been also depicted in Figure 3b, to get an insight of the chemical course of the reaction on physical grounds and hence to describe the entanglement features of this chemical process. As it might be observed from Figure 3b, we can distinguish three stages of the reaction in the passage from the **R** to the **TS**: (i) from the **R** region to $R_x \simeq -2$ wherein the atomic carbon (squares) gains charge to the expense of all the hydrogenic species, that is, the leaving (circles) and the ones (triangles) attached to carbon, whereas the entering hydrogenic species (diamonds) augments its charge smoothly up to the next stage, (ii) at $R_x \simeq -1$ the entering species gets it maximum charge (−1.0 a.u.) whereas the rest of the hydrogenic species become more negative and the atomic carbon looses its charge up to the next stage, and (iii) at $R_x \simeq -0.5$ the atomic carbon reaches a maximum charge deficiency where the entering and the leaving hydrogenic species equalize and start exchanging charge. It is interesting to mention that according to a classical information-theoretical analysis (see Ref. [54]) all this stages have been previously characterized by a BCER (at $R_x \simeq -2$), by a bond-breaking (B-B) region (at $R_x \simeq -1$), and by a charge transfer process (at $R_x \simeq -0.5$). Therefore, the two critical points observed at $R_x \simeq -1$ and +1 for the entanglement measures and the energy (see Fig. 3a) are associated to the transferring of charge process. Certainly, the **TS** is associated with the METS wherein it is evident that an equalization of charge occurs.

In Figure 3c, we have outlined the S_N2 reaction features according to the atomic potentials (a.u.). Three stages might be illustrated: (i) from the **R** to $R_x \simeq -2$ we might note a decrement for all the atomic $\in_i$ although the attached hydrogenic species (leaving hydrogen represented with circles, and the ones attached to carbon, triangles) show much larger values than the ones for the atomic carbon (squares) and the entering hydrogenic species (circles), hence providing the driving force of the reaction up to $R_x \simeq -1$, (ii) at this region the leaving atomic species and the hydrogenic ones attached to carbon equalize their potential, and (iii) finally at the third stage the entering hydrogenic species increases its potential whereas the leaving one shows an opposite behavior up to the **TS**,

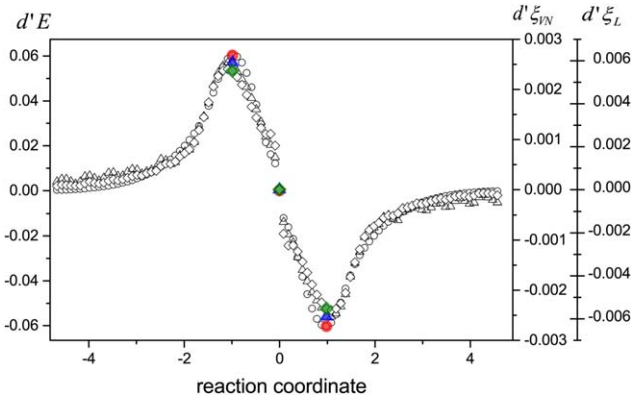

Figure 4. First derivative for the energy profile (circles) and the entanglement measures, linear (squares), and von Neumann (triangles) profile for the S_N2 reaction. To guide the eye, colored dots indicate the critical points: energy (red), linear (blue), and von Neumann (green).

where the potentials get equalized. At this region, the rest of the atomic species (carbon and the attached hydrogens) show a maximum local potential. It is worthy to mention that all these stages have been characterized by classical information-theoretic measures (see Ref. [54]), that is, the BCER, the bond-breaking (B-B) region and the **TS**. Therefore, the entanglement measures and the energy are associated with the electric potentials through the same features discussed above, at $R_x \simeq -1$ and $+1$, that is, the two inflection points are linked to the B-B process. Besides, from Figure 3c, we also observed that an equalization of the atomic potentials of leaving hydrogen (diamonds) and the ones attached to the carbon atom (squares) before the **TS**. Afterward, we similarly observe the equalization of the electric potentials between the entering hydrogen (circles) and the attached to carbon hydrogens (triangles). Therefore, the inflection points of the entanglement measures can be associated to these concurrent process. It is important to note that both, the **TS** and the **METS** occur at the same region and it is due to the equalization of both, charges and electric potentials of the entering and the leaving hydrogens, this process explain the maximum entropy for the mixed states.

As in the case of the previous reaction, we have found useful to depict the derivatives of these measures along with the energy in Figure 4, so as to analyze their critical points. Note that both quantum information-theoretic quantities hold two inflection points at $R_x \simeq -1$ and $+1$, that is, changes in the slopes of the curves are apparent. This has also been observed from the energy profile (see Fig. 3a).

In Table 2, we have reported the values for all the chemically significant intermediates (**R**, **P,** and **TS**) that are readily apparent from the entropies and the entanglement measures [Eqs. (15–18)] at the CISD/6–311++G** level of theory.

Three center insertion reaction of Silylene

The $SiH_2+H_2 \rightarrow SiH_4$ represents the silylene insertion reaction into hydrogen. This reaction occurs in two stages as depicted in Figure 5: a three-center bond is formed through the electrophilic attack from the silylene into the H···H molecule (before the **TS**) followed by a nucleophilic interaction from the H···H to the silylene which produces the **TS** to finally form the product. Accordingly, it is useful to distinguish both entering hydrogens of H···H: in the electrophilic stage as the $H_{electro}$, standing for the hydrogenic species attaching to the Silylene complex before the **TS**, and in the nucleophilic stage as the H_{nucleo}, standing for the one that attaches into the new Silylene complex after the **TS**.

The intrinsic reaction path (IRC) for the three center insertion reaction $SiH_2+H_2 \rightarrow SiH_4$ was obtained at the MP2/6–31G(d,p) level of theory which produced and IRC path of 72 points evenly distributed among the reaction path.[57] Then, the CISD/6–311++G** method was used[56] for determining all the chemical structures at the IRC and hence all their corresponding quantum information-theoretic quantities and physical properties (q_i and $\in_i$). The energy profile, along with the entanglement measures are drawn in Figure 6a.

It is observed, from Figure 6a, the resemblance among both quantum information-theoretic and the energy profile which shows a small energy barrier in passing from **R** through **P**. In connection with the latter, it is worth noting that METS do not coincide with that of the energy profile (TS), that is, at $R_x = 0$ the critical points of the quantum information-theoretical values appear slightly shifted in the direction of the products; moreover, despite the fact that both (TS and METS) are located in the transition region, the **TS** is not associated to the physical situation indicated by the phenomenological behavior of the reaction according to the evidence provided by the atomic charges and atomic electric potentials (see Figs. 6b and 6c). This is not surprising as the topological meaning of the **TS** as the first order saddle point of the energy profile is not expected to match necessarily with any physical phenomena, other than concoursing with the transition vector in the passage from reactive to products. In contrast, the **METS** signals to the region of charge transferring among the silicon atom and the hydrogenic species, in particular $H_{nucleo} \rightarrow Si$. We believe that the latter conforms a very robust argument to provide with physical significance to the **METS** as this is what one would expect from a chemical transition (mixed state), where some of the physical properties become equalized. In

Table 2. Linear and von Neumann entropies and the associated entanglement measures corresponding to **R**, **P,** and **TS** for the S_N2 reaction according to Eqs. (15)–(18).

	S_L	ξ_L	S_{vN}	ξ_{vN}
R	9.1895718 E − 01	2.7463488 E − 02	1.8800486 E + 00	8.8265752 E − 02
P	9.1895718 E − 01	2.7463488 E − 02	1.8800486 E + 00	8.8265752 E − 02
TS	9.1927889 E − 01	3.1339357 E − 02	1.8897769 E + 00	9.8009921 E − 02

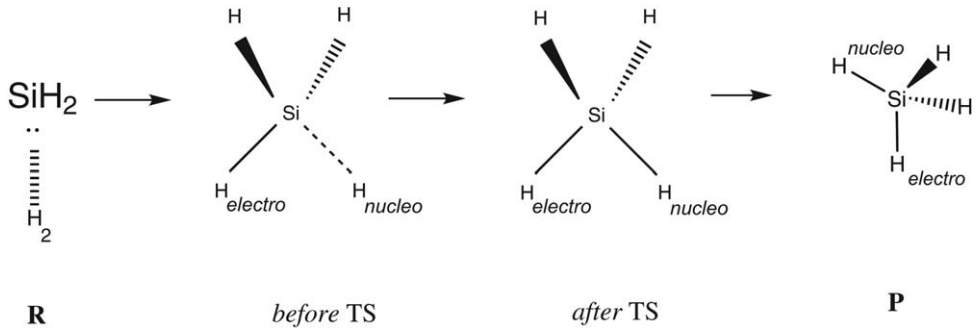

Figure 5. Stationary points of the Silylene insertion reaction into H_2 along the path: the prereaction complex, the transition state structure (TS) and the product.

this sense, it might be of interest from future work to explore chemical equalization principles at the light of quantum entanglement.

In relation to this entanglement behavior, a physical explanation is in turn. To this end, we have used the atomic charges of the atomic species at the path of the three insertion reaction of Silylene into H_2, which have been drawn in Figure 6b. As in the previous reactions, these atomic properties have proved to be useful to physically describe the chemical transformations at the IRC of the reaction. Accordingly, the atomic charges for the hydrogen atoms increase positively, while for the silicon one increases negatively at $R_x \simeq -1.0$. Both showing extrema at $R_x \simeq -0.4$, where the bond-forming ($Si \cdots H_{electro}$) and bond-breaking ($H_{electro} \cdots H_{nucleo}$) processes get completed.[56] A complementary analysis is provided by the atomic electric potentials, depicted in Figure 6c, which reveals that hydrogenic species increases (negatively) while the silicon atom decreases (negatively), indicating that at the onset of $R_x \simeq -1.0$, the bond forming/breaking processes (above referred) have initiated, up to a critical point where the atomic potentials for $H_{electro}$ (triangle down) and Si (square) hold extrema, at $R_x \simeq -0.4$, where the processes get completed. Hence, the electric potential difference (maximum to minimum, for $H_{electro}$ and Si, respectively) becomes the largest before the **TS**. That is, whereas the Si atom shows minimum capacity to acquire charge, the $H_{electro}$ atom shows its maximum capacity (it is called an electrophilic interaction, see above). Note in Figure 6b that Si atom shows maximum negative charge and $H_{electro}$ shows its maximum positive charge at the chemical path. This electrostatic situation marks the end of the bond rupture ($H_{electro} \leftrightarrow H_{nucleo}$) and the bond forming ($Si \rightarrow H_{electro}$) processes before the **TS**, and these are

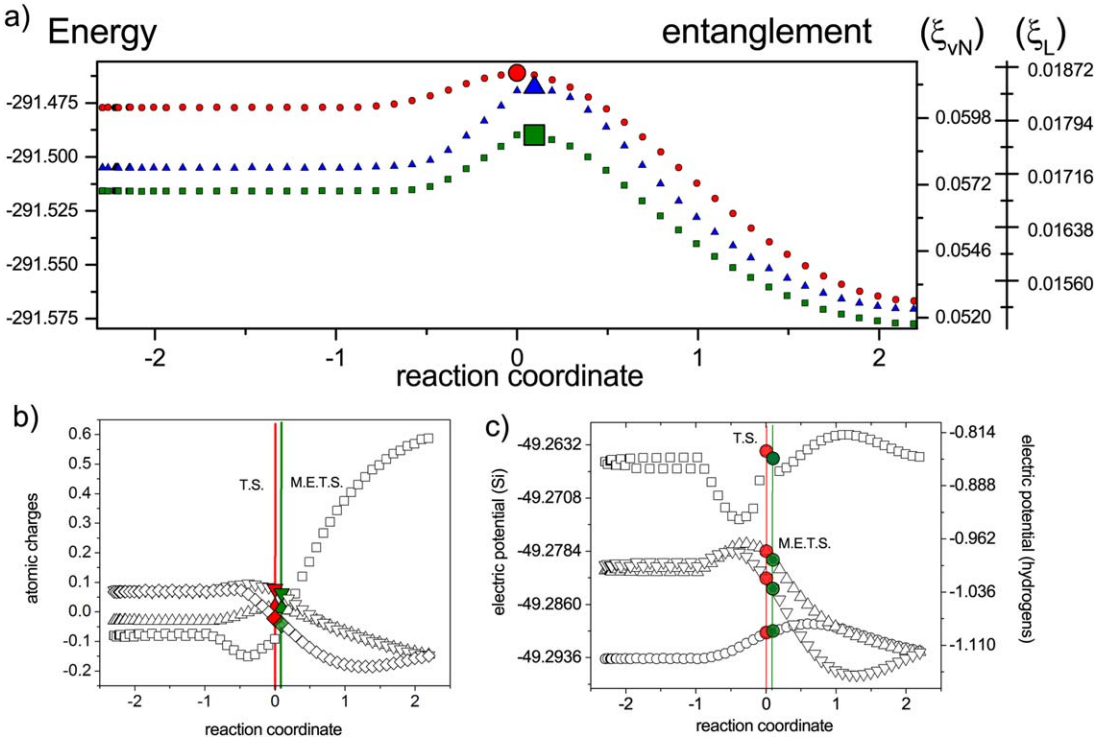

Figure 6. Phenomenological behavior for a) the energy (red) at the **TS** and for the entanglement measures (linear in blue, and von Neumann in green) at the **METS** according to b) the atomic charges (q_i) and c) atomic electric potentials ($\in_i$) for the insertion reaction of Sililene: Silicon(squares), $H_{electro}$ (triangle down), H_{nucleo} (diamond), H – H attached to silicon (triangle up).

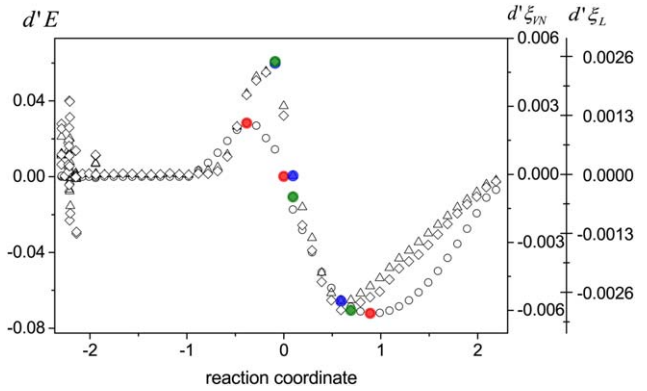

Figure 7. First derivative for the energy profile (circles) and the entanglement measures, linear (squares), and von Neumann (triangles) profile for the three insertion reaction of Silylene into H_2. To guide the eye, colored dots indicate the critical points: energy (red), linear (blue), and von Neumann (green).

responsible for the behavior of the entanglement measures (see Fig. 6a). Please note that at the onset of $R_x \simeq -0.4$ the entanglement start increasing once the two initial species, SiH_2+H_2, approach enough to react and becoming a single chemical species, called chemical adduct o reactive complex. Apparently, this situation ends at the **TS**, however, it is very interesting to note that physically the largest interaction between the atomic species occur slightly later, after the **TS**, at $R_x \simeq 0.2$, where the charge exchange between the Si and all the hydrogenic species take place. Therefore, it is apparent that the largest interactions between the species occur at the maximum mixing, that is, at the **METS**, which is reflected by the quantum measures (see Fig. 6a). Conversely, it is apparent that the inflection point observed for the entanglement measures before the **METS** is mainly due to equalization of charge at $R_x \simeq 0$ between the $H_{electro} \leftrightarrow H_{nucleo}$).

In the last stage, when the nucleophilic process is at place (see above), the opposite phenomenon occurs, that is, as the Si species looses charge after the TS, the H_{nucleo} becomes more negative (see Fig. 6b) and then the bond forming process occurs ($H_{nucleo} \rightarrow Si$), which is in the opposite direction of that occurring in the electrophilic stage above ($Si \rightarrow H_{electro}$). It is worth observing that as the Silicon atomic species looses charge and the atomic potentials of the entering hydrogens decrease, the entanglement measures (Fig. 6a) are more influenced by the later and decrease monotonically from the **METS** to the **P** until the bond forming $H_{nucleo} \rightarrow Si$ is reached, then the entanglement measures decrease less rapidly, indicating also the interacting aspects of the quantum correlation measures. As in the first stage of the reaction, it is apparent that the inflection point observed for the entanglement measures afterward the **METS** is mainly due to equalization of charge between the $H_{electro}$ and the H – H attached to silicon in the region 0.5 to +1.

As in the case of the previous reactions, we have found useful to plot the derivatives of these measures along with the energy in Figure 7, so as to analyze the physical origin of the critical points. Note from the figure that both quantum information-theoretic quantities hold two inflection points at $R_x \simeq 0$ and between 0.5 and +1, that is, where changes in the slopes of the curves are apparent. This is also observed for the energy profile, where its critical points although, are shifted as compared with those of the entanglement measures (see Fig. 7). It is interesting to note, as mentioned earlier, that maxima of the energy (TS) and for the entanglement measures (METS) are also slightly shifted. As we aforementioned, the physical meaning of the critical points might be understood through the phenomenological behavior of the charges.

In Table 3, we have reported the values for all the chemically significant intermediates (**R**, **P,** and **TS**) along with the adduct associated to the **METS** (see above) that are readily apparent from the entropies and the entanglement measures [Eqs. (15) and (18)] at the CISD/6–311++G** level of theory.

Diels–Alder cyclopentadiene with maleic anhydride reaction (exocycloadduct)

The Diels–Alder reaction is an important addition reaction in organic chemistry. The reaction involves the cycloaddition of a conjugated diene with an alkene to form a compound containing a six-membered ring. A unique type of stereoselectivity is observed in Diels–Alder reactions when the diene is cyclic. In the reaction of maleic anhydride with cyclopentadiene, which might produce two different cycloadducts: cys-5-norbornene-2-3-endo/exo-dicarboxylic anhydride (see Fig. 8), the endo isomer is formed experimentally rather than the exo isomer, which is the one that is thermodynamically favored. It is well-known that most Diels–Alder reactions between simple reactants lead preferentially to the endo adduct.[58] However, the reason for such behavior has become the subject of great debate in recent years.[59] In this study, we will present results for the exocycloadduct only, information-theoretical arguments for the endo preference will be discussed elsewhere.[60]

The intrinsic reaction path (IRC) for the exocycloadduct of the Diels–Alder reaction above referred was obtained at the B3LYP/6–311+G** level of theory which produced and IRC path of 46 points evenly distributed among the reaction

Table 3. Linear and von Neumann entropies and the associated entanglement measures corresponding to **R**, **P,** and **TS** for the three insertion reaction of Silylene into H_2 according to Eqs. (15)–(18).

	S_L	ξ_L	S_{vN}	ξ_{vN}
R	9.4540252 E − 01	1.7242577 E − 02	2.2541642 E + 00	5.6936841 E − 02
P	9.4528756 E − 01	1.5177253 E − 02	2.2489734 E + 00	5.1749958 E − 02
TS	9.4546529 E − 01	1.8373566 E − 02	2.2563515 E + 00	5.9125265 E − 02
METS(adduct)	9.4546782 E − 01	1.8417475 E − 02	2.2563563 E + 00	5.9128376 E − 02

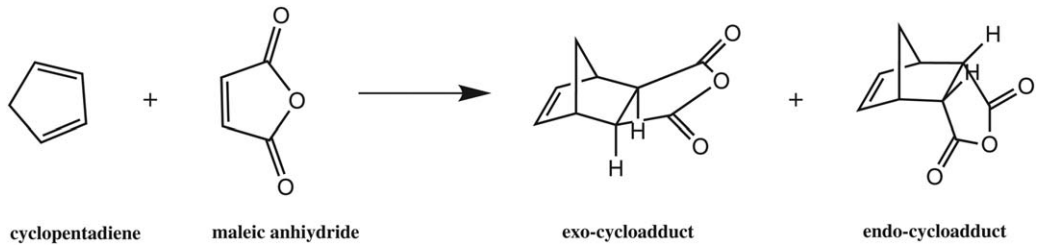

Figure 8. The Diels–Alder cycloaddition reaction of cyclopentandiene into maleic anhydride. Two cycloadducts are produced: exo (favored thermodynamically) and endo (experimentally observed).

path.[60] Then, the CISD/6–311+G* method was used for determining all the chemical structure at the IRC and hence all their corresponding quantum information-theoretic quantities and physical properties (q_i and $\in_i$). The energy profile for this reaction is depicted in Figure 9a, along with both entanglement measures, linear and von Neumann, for the for the Diels–Alder addition reaction of cyclopentandiene into maleic anhydride. Note that both, the **TS** and the **METS**, possess maxima at different locations at the path of the IRC. As it was discussed for the previous reaction, some comments are pertinent: the **TS** is not associated to the physical situation indicated by the phenomenological behavior of the reaction according to the evidence provided by the atomic charges and the electric potentials. In contrast, the **METS** indicates the maximum electric potential difference between the molecular species (maleic and ciclotentadyene). This concurrent process reveals a bonding situation between the molecular complexes revealing a different mechanism for this reaction as compared with the previous ones discussed above.

Most of Diels–Alder reactions proceed in only one concerted step involving the simultaneous formation of the two new single bonds appearing in the product (see Fig. 8). This mechanism is reflected in the information-theoretical measures for this reaction.

The essential features that might be distinguished from the entanglement measures comprehend three regions: (i) from the **R** up to the **TS/METS** (note that the maximum entangled state is slightly shifted toward the **P** as in the last reaction, see hydrogenic abstraction reaction subsection), and (ii) from this critical point up to $R_x \simeq -5$ where the entanglement measures become constant. These observations can be associated to physical phenomena through the atomic charges (Fig. 9b) and atomic electric potentials (Fig. 9c). There is a global process of charge exchanging between the chemically meaningful molecular species among the different stages, that is, (i) in the first

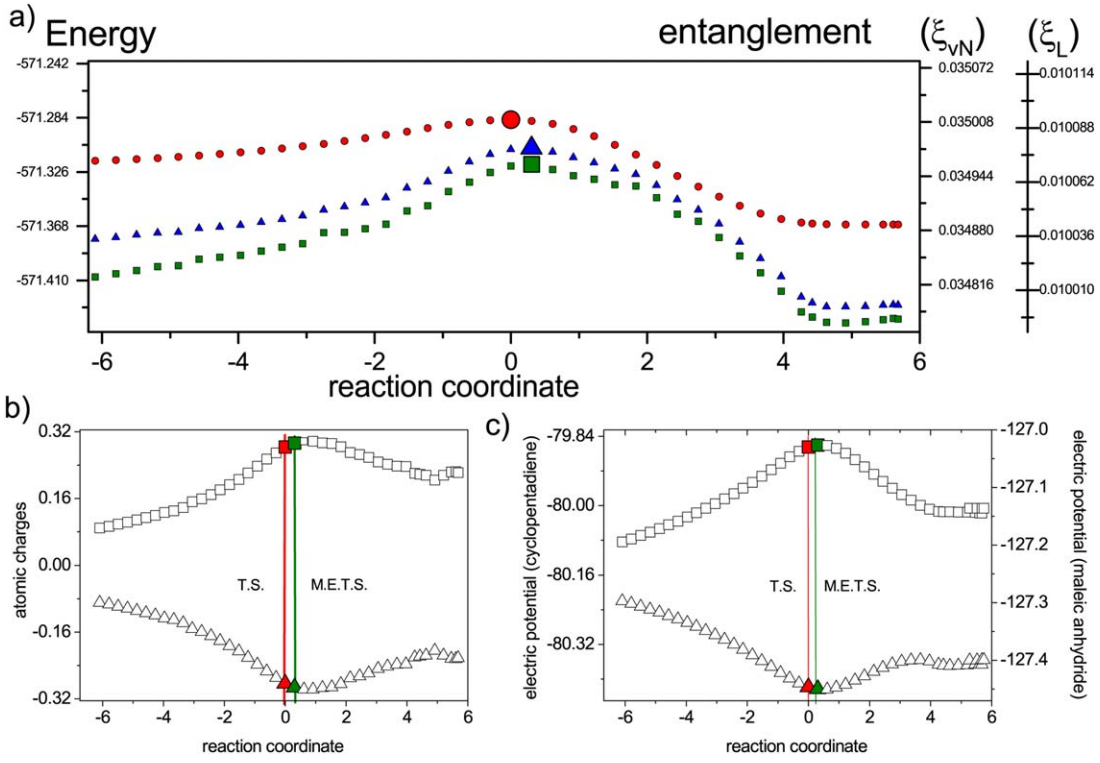

Figure 9. Phenomenological behavior for a) the energy (red) at the **TS** and for the entanglement measures (linear in blue, and von Neumann in green) at the **METS** according to the molecular electric potential (below) for the Diels–Alder addition reaction of cyclopentandiene (triangles, left scale) into maleic anhydride (squares, right scale).

Table 4. Linear and von Neumann entropies and the associated entanglement measures corresponding to **R**, **P,** and **TS** for the Diels–Alder addition reaction of cyclopentandiene into maleic anhydride according to Eqs. (15)–(18).

	S_L	ξ_L	S_{vN}	ξ_{vN}
R	9.8848875 E − 01	1.0033128 E − 02	3.7960180 E + 00	3.4818231 E − 02
P	9.8848840 E − 01	1.0002857 E − 02	3.7959699 E + 00	3.4770512 E − 02
TS	9.8848930 E − 01	1.0080132 E − 02	3.7961549 E + 00	3.4955439 E − 02
METS	9.8848932 E − 01	1.0081073 E − 02	3.7961628 E + 00	3.4962501 E − 02

region (from the $R_x \simeq -2$ to the **TS**) the transfers charge in favor of the cyclopentadiene and (ii) the process gets reversed and the cyclopentadiene (CP) transfers charge to the maleic anhydride (MA) up to $R_x \simeq -4$ and then charge stabilization is reached (Fig. 9b). This behavior is reflected by the molecular electric potentials (depicted at Fig. 9c) which signal two main stages: (i) reaction starts by the driving force provided by the molecular electric potentials at the **R** where the MA holds a minimum value whereas the CP possesses a maximum, as the reaction progresses and the molecular species approach to each other a maximum interaction is reached at the **METS**, and hence (ii) a new driving force acts in the opposite direction from the CP to the MA. This oscillating force ends when the reactions gets completed at the **P**. Once again, it is worth noting, (as it happened in the previous analyzed reaction, see three center insertion reaction of silylene subsection), that the maximal interaction of the molecular species, according to atomic electric potentials (Fig. 9c), occurs at the **METS** and not at the **TS**. It is difficult to associate this behavior to numerical noise due to the remarkable agreement between the phenomenological interaction among species and the **METS**.

Entropy and entanglement values, Eqs. (15–18), calculated at the CISD/6–311+G* level of theory have been reported in Table 4 for all the chemically significant intermediates (**R**, **P,** and **TS**) along with the adduct associated to the **METS** (see above).

Correlation energy and entanglement

Previous studies have suggested a relation of correlation energy with the von Neumann entropy. Indeed, Esquivel et al[61] and Ramírez et al.[62] examined the implications of the Collins conjecture[63] to show numerically that for three-electron atoms and some selected small molecules, the von Neumann entropy behaves linearly with the correlation energy as the quality of the wave function increases. Moreover, Huang and Kais[64] and Hofer[65] have used entanglement as an alternative measure of electron correlation for helium-like systems.

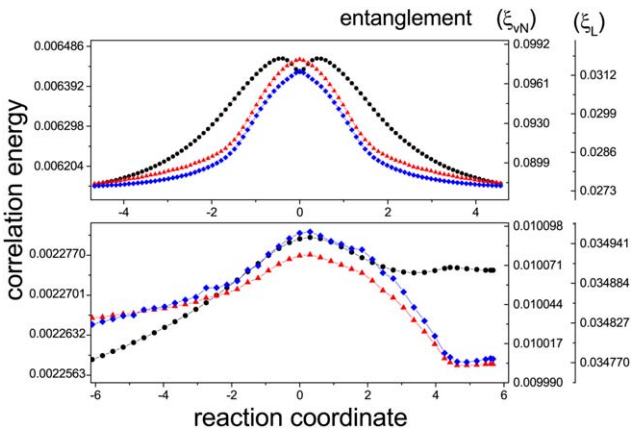

Figure 10. Correlation energy (in black) and the entanglement measures, linear (blue), and von Neumann entropies (red) for the S_N2 (top) and for the Diels–Alder (bottom).

It is known[68,69] that a wave function composed of a single Slater determinant does not content quantum correlations usable as a resource for quantum information tasks, implying that the Hartree–Fock wave function does not represent an entangled state, whereas the multideterminantal wave functions used in post-HF methods are endowed with entanglement. The later implies that the nonlocal effect linked to entanglement must be present in any post-HF wave function independently of its quality.

In this section, we have found useful to analyze the possible link between the correlation energy and entanglement. This is represented in Figure 10 for the hydrogenic nucleophilic substitution (top) and the Diels–Alder addition reaction of cyclopentandiene into maleic anhydride (bottom).

From Figure 10, we have learned that correlation energies possess a different profile to that of the entanglement measures. Therefore, it seems that Collin's conjecture[63] only applies for the ground state of atomic and molecular systems. For excited states and for the chemical course of reactions more studies should be undertaken.

Conclusions

In this work, we have studied the quantum information features through the linear and von Neumann entanglement measures of selected elementary chemical reactions: hydrogenic abstraction, nucleophilic hydrogenic substitution, three-atom insertion reaction of silylene into hydrogen, and the cycloaddition of cyclopentadiene into anhydride maleic. To associate physical features to the entanglement profiles, we have performed a phenomenological analysis of the chemical processes in the passage from reactive to products through the transition region. This is achieved through the most indicative descriptors of de molecular densities: the atomic charges and the electric potentials.

The main features of the entanglement measures as the chemical reaction evolves can be briefly indicated as follows: at the **R/P** regions the reactants/products consist of specific chemical species showing the lowest values of entanglement, indicating a chemical situation of separable states: reactives and products. Afterward, entanglemet profiles show inflection

points, reflecting physical situations of charge/potential equalization. At the transition region, **TS** and **METS** represent the same region for symmetrical reactions (hydrogenic abstarction and nucleophilic substitution), for the nonysymmetrical (three center insertion and Diels–Alder) the **TS** only reflects its topological origin, disregarding of any physical significance. In contrast, the **METS** completely reveals the mixed state nature of the activated complex that represents the chemical situation defined by IUPAC (http://goldbook.iupac.org/T06468.html): "the TS of an elementary reaction is that set of states (each characterized by its own geometry and energy) in which an assembly of atoms, when randomly placed there, would have an equal probability of forming the reactants or of forming the products of that elementary reaction." We have shown in this work that it is through the quantum-information concept represented by the **METS** that such a chemical situation is fully described. Let us remember that the mathematical definition of the **TS** through the first-order saddle point does not necessarily hold any chemical significance. Work is in progress in our laboratories to characterize other more complex reactions.

The chemical process involves the transformation from quasi-independent subsystems at the **R/P** characterized by smaller and non-zero quantum entropies to reach the maximum entangled TS characterizing highly correlated subsystems in a mixed state. Besides, other critical points are observed from the entanglement profiles at the vicinity of the transition region, indicating chemical situations of charge or potential equalization depending on the reaction under study. Most important, the observations of this paper lead us to associate the **METS** to a equiprobable states of maximum chemical reactivity which connects two or more states with lower entanglement through the PESs. Accordingly to the later, the chemical significance of **METS** discussed on this work is guaranteed.

Acknowledgments

J.S.D. and A.R.P. belong to the Andalusian research group FQM-0207 and R.O.E. to FQM-020. Allocation of supercomputing time from Laboratorio de Supercómputo y Visualización at UAM, Sección de Supercomputación at CSIRC Universidad de Granada, and Departamento de Supercómputo at DGSCA-UNAM is gratefully acknowledged.

Keywords: quantum entanglement · chemical reactions · molecular systems

How to cite this article: R. O., Esquivel, M., Molina-Espíritu, A. R., Plastino, J. S., Dehesa *Int. J. Quantum Chem.* **2015**, *115*, 1417–1430. DOI: 10.1002/qua.24926

[1] J. Pople, *Rev. Mod. Phys.* **1999**, *71*, 1267.
[2] C. E. Shannon, W. Weaver, The Mathematical Theory of Communication; University of Illinois Press: Urbana, **1949**.
[3] (a) Q. C. Shi, S. Kais, *Chem. Phys.* **2005**, *309*, 127; (b) Q. C. Shi, S. Kais, *J. Chem. Phys.* **2004**, *121*, 5611.
[4] C. Das, K. Bhattacharyya, *Phys. Rev. A* **2009**, *79*, 012107.
[5] S. Liu, *J. Chem. Phys.* **2007**, *126*, 191107.
[6] A. Nagy, *Chem. Phys. Lett.* **2007**, *449*, 212.
[7] R. O. Esquivel, J. C. Angulo, J. S. Dehesa, J. Antolín, S. López-Rosa, N. Flores-Gallegos, M. Molina-Espíritu, C. Iuga, In Recent Advances Toward the Nascent Science of Quantum Information Chemistry in Information Theory: New Research, Chapter *8*; P. Deloumeaux, J. D. Gorzalka, Eds.; Nova Science Publishers, Hauppage, NY, **2012**; pp. 297–334.
[8] R. O. Esquivel, N. Flores-Gallegos, C. Iuga, E. M. Carrera, J. C. Angulo, J. Antolín, *Theor. Chem. Acc.* **2009**, *124*, 445.
[9] R. O. Esquivel, N. Flores-Gallegos, C. Iuga, E. M. Carrera, J. C. Angulo, J. Antolín, *Phys. Lett. A* **2010**, *374*, 948.
[10] R. O. Esquivel, M. Molina-Espíritu, J. C. Angulo, J. Antolín, N. Flores-Gallegos, J. Dehesa, *Mol. Phys.* **2011**, *109*, 2353.
[11] M. Tichy, F. Mintert, A. Buchleitner, *J. Phys. B: At. Mol. Opt. Phys.* **2011**, *44*, 192001.
[12] M. A. Nielsen, E. Knill, R. Laflamme, *Nature* **1998**, *396*, 52.
[13] (a) J. Al-Khalili, J. McFadden, *Life on the Edge: The Coming of Age of Quantum Biology*; Bantam Press, New York, **2014**, ISBN-13: 978–0593069318; (b) P. Ball, *Nature* **2011**, *474*, 272; (c) M. Arndt, T. Juffmann, V. Vedral, *HFSP J.* **2009**, *3*, 386; (d) J. A. Pauls, Y. Zhang, G. P. Berman, *Phys. Rev. E* **2013**, *87*, 062704; (e) J. Zhu, S. Kais, A. Aspuru-Guzik, *J. Chem. Phys.* **2012**, *137*, 074112.
[14] (a) O. Legeza, J. Solyom, *Phys. Rev. B* **2003**, *68*, 195116; (b) O. Legeza, J. Solyom, *Phys. Rev. B* **2004**, *70*, 205118; (c) J. Rissler, R. M. Noack, S. R. White, *Chem. Phys.* **2006**, *323*, 519.
[15] (a) Q. Wei, S. Kais, B. Friedrich, *J. Chem. Phys.* **2011**, *135*,154102; (b) H. F. Wang, S. Kais, *Chem. Phys. Lett.* **2006**, *421*, 338.
[16] S. Kais, *Adv. Chem. Phys.* **2007**, *134*, 493.
[17] (a) R. F. W. Bader, *Atoms in Molecules*; Oxford U.P.: New York, **1994**; (b) F. L. Hirshfeld, *Theor. Chim. Acta* **1977**, *44*, 129; (c) P. Ayers, *J. Chem. Phys.* **2000**, *113*, 10886.
[18] C. Amovilli, N. H. March, *Phys. Rev. A* **2004**, *69*, 054302.
[19] Z. Huang, S. Kais, *Chem. Phys. Lett.* **2005**, *413*, 15.
[20] Z. Huang, H. Wang, S. Kais, *J. Mod. Opt.* **2006**, *53*, 2543.
[21] G. Benenti, S. Siccardi, G. Strini, *Eur. Phys. J. D* **2013**, *67*, 1.
[22] Y. C. Lin, C. Y. Lin, Y. K. Ho, *Phys. Rev. A* **2013**, *87*, 022316.
[23] (a) R. J. Yañez, A. R. Plastino, J. S. Dehesa, *Eur. Phys. J. D* **2010**, *56*, 141; (b) D. Manzano, A. R. Plastino, J. S. Dehesa, T. Koga, *J. Phys. A: Math. Theor.* **2010**, *43*, 275.
[24] P. A. Bouvrie, A. R. Plastino, P. Sanchez-Moreno, J. S. Dehesa, *Eur. Phys. J. D* **2012**, *66*, 15.
[25] (a) J. S. Dehesa, T. Koga, R. J. Yañez, A. R. Plastino, R. O. Esquivel, *J. Phys. B: At. Mol. Opt. Phys.* **2012**, *45*, 015504; (b) J. S. Dehesa, T. Koga, R. J. Yañez, A. R. Plastino, R. O. Esquivel, *J. Phys. B: At. Mol. Opt. Phys.* **2012**, *45*, 239501; (c) Y. C. Lin, C. Y. Lin, Y. K. Ho, *Phys. Rev. A* **2013**, *87*, 022316.
[26] J. Pipek, I. Nagy, *Phys. Rev. A* **2009**, *79*, 052501.
[27] N. L. Harshman, W. F. Flynn, *Quantum Inf. Comput.* **2011**, *11*, 278.
[28] (a) P. Kościk, A. Okopińska, *Phys. Lett. A* **2010**, *374*, 3841; (b) P. Kościk, *Phys. Lett. A* **2011**, *375*, 458; (c) P. Kościk, *Phys. Lett. A* **2013**, *377*, 2393.
[29] H. Wang, S. Kais, *Isr. J. Chem.* **2007**, *47*, 59.
[30] R. G. Nazmitdinov, N. S. Simonovic, A. R. Plastino, A. V. Chizhov, *J. Phys. B: Atom. Mol. Opt. Phys.* **2012**, *45*, 205503.
[31] A. P. Majtey, A. R. Plastino, J. S. Dehesa, *J. Phys. A: Math. Theor.* **2012**, *45*, 115309.
[32] P. Sadhukhan, S. M. Bhattacharjee, *J. Phys. A: Math. Theor.* **2012**, *45*, 425302.
[33] S. Schröter, H. Friedrich, J. Madroñero, *Phys. Rev. A* **2013**, *87*, 042507.
[34] F. Carlier, A. Mandilara, A. Sarfati, *J. Phys. B: At. Mol. Opt. Phys.* **2007**, *40*, S199.
[35] O. Osenda, P. Serra, *Phys. Rev. A* **2007**, *75*, 042331.
[36] O. Osenda, P. Serra, *J. Phys. B: At. Mol. Opt. Phys.* **2008**, *41*, 065502.
[37] J. P. Coe, A. Sudbery, I. D'Amico, *Phys. Rev. B* **2008**, *77*, 205122.
[38] A. M. Gavrilik, Y. A. Mishchenko, *J. Phys. A: Math. Theor.* **2013**, *46*, 145301.
[39] C. L. Benavides-Riveros, J. M. Gracia-Bondía, M. Springborg, *Phys. Rev.* **2013**, *88*, 022508.
[40] C. L. Benavides-Riveros, J. M. Gracia-Bondía, J. C. Várilly, *Phys. Rev. A* **2012**, *86*, 022525.
[41] R. O. Esquivel, N. Flores-Gallegos, M. Molina-Espíritu, A. R. Plastino, J. S. Dehesa, J. C. Angulo, J. Antolín, *J. Phys. B: At. Mol. Opt. Phys.* **2011**, *44*, 175101.

[42] G. Barcza, O. Legeza, K. H. Marti, M. Reiher, *Phys. Rev. A* **2011**, *83*, 012508.
[43] M. Mottet, P. Tecmer, K. Boguslawski, Ö. Legeza, M. Reiher, *Phys. Chem. Chem. Phys.* **2014**, *16*, 8872.
[44] K. Boguslawski, P. Tecmer, G. Barcza, O. Legeza, M. Reiher, *J Chem. Theory Comput.* **2013**, *9*, 2959.
[45] O. Legeza, J. Solyom, *Phys. Rev. Lett.* **2006**, *96*, 116401.
[46] V. Murg, F. Verstraete, R. Schneider, P. R. Nagy, O. Legeza, *J Chem Theory Comput* **2015**, *11*, 1027.
[47] E. Fertitta, B. Paulus, G. Barcza, Ö. Legeza, *Phys. Rev. B* **2014**, *90*, 245129.
[48] (a) G. Ghirardi, L. Marinatto, *Phys. Rev. A* **2004**, *70*, 012109; (b) G. Ghirardi, L. Marinatto, T. Weber, *J. Stat. Phys.* **2002**, *108*, 49.
[49] A. R. Plastino, D. Manzano, J. S. Dehesa, *Europhys. Lett.* **2009**, *86*, 20005.
[50] J. Naudts, T. Verhulst, *Phys. Rev. A* **2007**, *75*, 062104.
[51] V. C. G. Oliveira, H. A. B. Santos, L. A. M. Torres, A. M. C. Souza, *Int. J. Quantum Inf.* **2008**, *6*, 379.
[52] (a) P. O. Löwdin, *Adv. Quantum Chem.* **1970**, *5*, 185; (b) P. O. Löwdin, *Phys. Rev.* **1955**, *97*, 1474; (c) P. O. Löwdin, H. Shull, *Phys. Rev.* **1956**, *101*, 1730.
[53] (a) H. Eyring, *J. Chem. Phys.* **1935**, *3*, 107; (b) E. Wigner, *Trans. Faraday Soc.* **1938**, *34*, 29.
[54] R. O. Esquivel, M. Molina-Espíritu, J. S. Dehesa, J. C. Angulo, J. Antolín, *Int. J. Quantum Chem.* **2012**, *112*, 3578.
[55] M. Breneman, K. B. Wiberg, *J. Comput. Chem.* **1990**, *11*, 361.
[56] M. J. Frisch, G. W. Trucks, H. B. Schlegel, G. E. Scuseria, M. A. Robb, J. R. Cheeseman, G. Scalmani, V. Barone, B. Mennucci, G. A. Petersson, H. Nakatsuji, M. Caricato, X. Li, H. P. Hratchian, A. F. Izmaylov, J. Bloino, G. Zheng, J. L. Sonnenberg, M. Hada, M. Ehara, K. Toyota, R. Fukuda, J. Hasegawa, M. Ishida, T. Nakajima, Y. Honda, O. Kitao, H. Nakai, T. Vreven, J. A. Montgomery, Jr., J. E. Peralta, F. Ogliaro, M. Bearpark, J. J. Hey, E. Brothers, K. N. Kudin, V. N. Staroverov, R. Kobayashi, J. Normand, K. Raghavachari, A. Rendell, J. C. Burant, S. S. Iyengar, J. Tomasi, M. Cossi, N. Rega, J. M. Millam, M. Klene, J. E. Knox, J. B. Cross, V. Bakken, C. Adamo, J. Jaramillo, R. Gomperts, R. E. Stratmann, O. Yazyev, A. J. Austin, R. Cammi, C. Pomelli, J. W. Ochterski, R. L. Martin, K. Morokuma, V. G. Zakrzewski, G. A. Voth, P. Salvador, J. J. Dannenberg, S. Dapprich, A. D. Daniels, A. P. Farkas, J. B. Foresman, J. V. Ortiz, J. Cioslowski, D. J. Fox, Gaussian 09, Revision C.1; Gaussian: Wallingford, CT, **2011**, 9.
[57] R. O. Esquivel, N. Flores-Gallegos, J. S. Dehesa, J. C. Angulo, J. Antolín, K. Sen, *J. Phys. Chem. A* **2010**, *114*, 1906.
[58] J. Sauer, R. Sustmann, *Angew. Chem. Int. Ed. Engl.* **1980**, *19*, 779.
[59] C. S. Wannere, A. Paul, R. Herges, K. N. Houk, H. F. Schaefer, P. V. R. Schleyer, *J. Comput. Chem.* **2007**, *28*, 344.
[60] M. Molina-Espíritu, R. O. Esquivel, M. Kohout, J. C. Angulo, J. A. Dobado, J. S. Dehesa, S. Lpez-Rosa, C. Soriano-Correa, *J. Mol. Mod.* **2014**, *20*, 1.
[61] R. O. Esquivel, A. L. Rodriguez, R. P. Sagar, M. Ho, V. H. Smith, Jr., *Phys. Rev. A* **1996**, *54*, 259.
[62] J. C. Ramírez, C. Soriano, R. O. Esquivel, R. P. Sagar, M. Ho, V. H. Smith, Jr., *Phys. Rev. A* **1997**, *56*, 4477.
[63] D. M. Collins, *Z. Nat.* **1993**, *48*, 68.
[64] S. Kais, *Adv. Chem. Phys.* **2007**, *1134*, 439.
[65] T. S. Hofer, *F. Chem.* **2013**, *1*, 1.
[66] G. Ghirardi, L. Marinatto, *Phys. Rev. A* **2004**, *70*, 012109.
[67] H. Wang, S. Kais, *Isr. J. Chem.* **2007**, *47* 59.
[68] S. Kais, Ed. Quantum Information and Computation for Chemistry: Advances in Chemical Physics, Vol. 154; **2014**. (ISBN: 9781118495667).
[69] J. Naudts, T. Verhulst, *Phys. Rev. A* **2007**, *75*, 062104.

Received: 7 October 2014
Revised: 21 March 2015
Accepted: 6 April 2015
Published online 27 April 2015